ISSN 0869-5911, Petrology, 2009, Vol. 17, No. 2, pp. 138–157. © Pleiades Publishing, Ltd., 2009.
Original Russian Text © S.A. Silantyev, M.V. Mironenko, A.A. Novoselov, 2009, published in Petrologiya, 2009, Vol. 17, No. 2, pp. 154–174.

Hydrothermal Systems in Peridotites of Slow-Spreading Mid-Oceanic Ridges. Modeling Phase Transitions and Material Balance: Downwelling Limb of a Hydrothermal Circulation Cell

S. A. Silantyev, M. V. Mironenko, and A. A. Novoselov

Vernadsky Institute of Geochemistry and Analytical Chemistry, Russian Academy of Sciences, ul. Kosygina 19, Moscow, 119991 Russia

e-mail: silantyev@geokhi.ru

Received November 15, 2007; in final form, January 21, 2008

Abstract—A model is development for the kinetic and thermodynamic simulation of the interaction of seawater and its metamorphosed derivatives with crustal rocks in slow-spreading ridges. The thermodynamic modulus of the model is based on the GEOCHEQ complex, which makes it possible to simulate equilibria in systems of aqueous solutions–minerals–gases. The calculating code was modified and adjusted for the thermodynamic–kinetic simulation of the passage of irreversible solution–rock reactions with time. The simulations were carried out for a simplified crustal vertical section of slow-spreading (Hess-type) ridges, which consist only of mantle peridotites (spinel harzburgites). The results of our simulations demonstrate that the degree of peridotite serpentinization under the effect of low-temperature seawater when the rocks are exposed at the seafloor surface remains very low even after 10000 years of interaction. Serpentinization becomes efficient only at temperatures of 130–150°C at crustal depths of 3.5–4.5 km. The results of our simulations allowed us to develop a thermodynamic model for the origin of hydrothermal systems in peridotites in slow-spreading ridges, with regard for the major stages in the material and tectonic evolution of the Hess crust.

DOI: 10.1134/S0869591109020039

INTRODUCTION

The composition of the lithosphere generated in slow- and ultraslow-spreading mod-oceanic ridges (MOR) testifies that the geodynamic regime responsible for the development of these planetary-scale structures is unusual, as is manifested in the physicochemical parameters of the magmatic, metamorphic, and hydrothermal processes that form rock complexes in these structures and the parameters of related hydrothermal manifestations over vast areas of the oceanic basement in the basins of the Atlantic, Indian, and Arctic oceans.

Oceanic slow-spreading ridges are characterized by widespread extensive exposures of peridotites in the axial zones (including the walls of the rift valleys), with these peridotites being an inherent constituent of the Hess oceanic crust. The striking differences between the vertical sections of the crust of this type and normal (Penrose-type) crustal sections in the axial zones of fast-spreading centers (such as the East Pacific Rise) predetermine the geochemical specifics of processes participating in the generation of rock complexes and related hydrothermal manifestations in the global system of slow- and ultraslow-spreading MOR. Because exposures of mantle peridotites are widespread in the crest zone of slow-spreading MOR, the interaction of these rocks with seawater and its hydrothermal derivatives affects planetary geochemical cycles and the material balance in the hydrosphere–lithosphere system. Inasmuch as the Hess-type crust is the most primitive type of the oceanic crust, the rock complexes composing it and the related hydrothermal ore mineralization can be utilized as reference objects in reproducing the conditions of petrogenesis during the initial evolutionary stages of oceanic basins and the early stages of the development of the Earth's lithosphere as a whole. The turn of the 21st century has opened a new page in studying hydrothermal systems at MOR and exploring the related problem of the origin of life on the Earth. The 2001 cruise of the R/V *Atlantis* (United States) in the intersection area of the Mid-Atlantic Ridge (MAR) and Atlantis Fracture Zone (30°N) resulted in the discovery of the Lost City hydrothermal field, at which with hydrothermal vents are inhabited by microorganisms (*Archea* and *Eubacteria*) that are though to have been typical of the Earth's most ancient Hadean ocean (4.5–3.9 Ga) (Kelley et al., 2001). It was then determined that the geochemical specifics of this hydrothermal field are predetermined by its restriction to the Atlantis massif of ultramafic rocks, the largest one in the Central Atlantic (Kelley et al., 2005). Since this time, the vertical section of the oceanic crust of the Hess type has been viewed as one of the most possible crustal material of the ancient Earth that participated in ecosystems in which life has germinated on the Earth

(see, for example, Kelley et al., 2001, 2005; Alt and Shanks, 2003; Allen and Seyfried, 2004).

The main task of our research was the kinetic–thermodynamic simulation of interaction between seawater or its metamorphosed fluid derivatives and the crust of slow-spreading mid-oceanic ridges (MOR). Our simulations were carried out in order to elucidate the following problems: (1) the succession of phase transitions in peridotites during their interaction with seawater-derived fluid during its percolation through the oceanic crust, (2) the principal tendencies in the compositional evolution of the hydrothermal fluid, and (3) the time needed to effectively serpentinize rocks at slow-spreading mid-oceanic ridges.

CURRENT VIEWS ON HYDROTHERMAL SYSTEMS IN THE ULTRAMAFIC ROCKS OF SLOW-SPREADING RIDGES

In the late 1980s to early 1990s, extended (up to a few hundred kilometers long) exposures of mantle residue peridotites were discovered in the MAR crest zone of (Rona et al., 1987; Silantyev et al., 1991; Cannat et al., 1997), with these exposures found not only within transforms but also in the walls of the rift valley. Simultaneously the very first evidence was derived that a new type of MOR hydrothermal systems exists in relation to peridotites in slow-spreading ridges (Rona et al., 1987; Charlou et al., 1988). It was established that hydrothermal systems circulating in peridotites in the Hess crust can be discovered based on their unusual geochemical characteristics (anomalously high contents of CH_4 and low Mn concentrations in the bottom water) (Charlou et al., 1988, 2002, 2005; Bougault et al., 1993). Further research has demonstrated that hydrothermal systems related to ultramafic rocks are also typically bear a certain characteristic association of ore minerals (Bortnikov et al., 1994; Bogdanov et al., 2002; Barriga, 2002; Vikent'ev, 2004).

The geochemical and mineralogical characteristics of hydrothermal systems related to the Hess crust were discussed in a number of comprehensive reviews (see, for example, Bogdanov et al., 2002; Marques et al., 2006), which quote empirical data that pertain mostly to the composition and physicochemical parameters of the hydrothermal solutions and ore material precipitating from them. At the same time, there is still no synthetic kinetic–thermodynamic model for such hydrothermal systems.

As was mentioned above, hydrothermal systems in the Hess crust are marked by significant methane anomalies and differ from hydrothermal systems that circulate within the basaltic layer in having no accompanying Mn and He anomalies. It is commonly though that methane and hydrogen are actively generated in hydrothermal systems of the Hess crust in direct relation to the serpentinization of mantle peridotites (Bougault et al., 1993; Charlou et al., 1988) according to the reactions $6Ol + 7H_2O = 3Srp + Mag + H_2$ and $CO_2 + 4H_2 = CH_4 + 2\,H_2O$.[1] Results of the experimental study of olivine serpentinization at 300°C and 0.5 kbar demonstrate that serpentine synthesis is associated with the reduction of CO_2. This highlights the important role played by peridotites in the generation of abiogenic hydrocarbons (Berndt et al., 1996). The data quoted in this publication indicate that the transition of Fe^{2+} into Fe^{3+} in magnetite during serpentinization is associated with the release of H_2 and the transformation of dissolved CO_2 into reduced carbon-bearing compounds, including methane, ethane, and propane. According to (Berndt et al., 1996), magnetite serves as a catalyst phase for methane release in the course of serpentinization and facilitates and activates methane synthesis according to the well-known Fischer–Tropsch mechanism, in which the principal reactants are H_2 and CO_2. Some researchers believe that the release of vast hydrogen and methane volumes during the serpentinization of ultramafic rocks corresponds to the initial stage of the origin of oil and gas fields (see, for example, Charlou et al., 2005).

The first attempts to thermodynamically simulate the transformation of oceanic ultramafic rocks under the effect of seawater percolating through these rocks were made in (Silantyev et al., 1992). These researchers have constrained the temperature boundaries of discrete serpentinization stages and presented evidence that the phase composition of serpentinized peridotites is controlled mostly by the R/W ratio (rock/water mass ratio). Our later simulations (Silantyev et al., 2003) allowed us to demonstrate that the hydration of the Hess crust within the depth range from the seafloor surface to a depth of approximately 6 km can occur at various redox regimes: (1) strongly oxidizing (near the surface), which produces the aragonite + goethite association; (2) moderately oxidizing (fluid-dominated), whose characteristic mineral assemblage is serpentine + chlorite + hematite + pyrite (magnetite–hematite buffer); and (3) reduced rock-dominated, with the mineral assemblage serpentine + olivine + magnetite + pyrrhotite (QFM buffer). Silantyev et al. (2003) suggested that differences in the fluid regimes responsible for the dehydration of peridotites in the oceanic crust are controlled, first of all, by the bulk composition of the pristine rocks, with this composition predetermining the differences in the buffer characteristics of the rocks.

A similar scenario for the evolution of redox conditions in hydrothermal systems developing in ultramafic rocks was outlined in (Grichuk, 2005). The results of the numerical simulation carried out in that research

[1] Mineral symbols: *Act*—actinolite, *Amph*–amphibole, *Arg*—aragonite, *Atg*—antigorite, *Brc*—brucite, *Chl*—chlorite, *Ctl*—chrysotile, *Di*—diopside, *Dol*—dolomite, *Fa*—fayalite, Fe-*Act*—Fe-actinolite, *Fo*—forsterite, *Gt*—goethite, *Hem*—hematite, *Mag*—magnetite, Mg-*Sap*—Mg-saponite, Na-*Sap*—Na-saponite, *Ol*—olivine, *Py*—pyrite, *Po*—pyrrhotite, *Sap*—saponite, *Spl*—spinel, *Srp*—serpentine, *Tlc*—talc, *Tr*—tremolite.

demonstrate that seawater percolation through peridotites at temperatures of 350–370°C is associated with the successive development of the following three mineral assemblages: serpentine + brucite + chlorite + actinolite + magnetite, serpentinite + talc + chlorite + actinolite + magnetite + pyrite, and serpentine + talc + chlorite + pyrite + hematite + anhydrite. At contact with the first assemblage, reduced solutions are generated (Grichuk, 2005) that have high concentrations of Ca, H_2, and CH_4.

A thermodynamic model for the hydrothermal transformation of the lower part of the oceanic crust was proposed in (McCollom and Shock, 1998). This model takes into account petrological and geochemical aspects of interactions between seawater-derived fluid and olivine gabbro, gabbronorite, and troctolite at a temperature of 300–900°C. An important advantage of the model (McCollom and Shock, 1998) is the validation (based on the results of numerical simulations) of the phenomenon of high-temperature (≥700°C) interaction of seawater-derived fluid with deep oceanic rocks, a process that was earlier studied based on mineralogical and experimental (data on fluid inclusions) data (Kelley and Delaney, 1987; Silantyev, 1998).

The material balance and heat generation related to the serpentinization of peridotites at the Rainbow and Lost City hydrothermal fields (at MAR) were considered in (Allen and Seyfried, 2004). The calculation of the heat balance led these researchers to conclude that the exothermal character of the hydration reactions of olivine does not any significantly affect the thermal regime in the Hess crust. At the rainbow field, where the reaction zone near the seafloor surface hosts high-temperature (up to 400°C) emanations of hydrothermal solutions, the likely main factor controlling the thermal regime is magmatic activity at the roots of the circulation system. The results of geochemical simulations for the Lost City hydrothermal system permit higher temperatures in the reaction zone than those measured there in situ (40–90°C). Hence, the exothermal effect of the serpentinization reaction cannot be regarded as the main heat source for hydrothermal systems associated with peridotites. It is more probable that the rheology of the system and tectonic processes typical of crustal rocks in slow-spreading ridges are favorable for the deep penetration of seawater into the still-hot oceanic lithosphere (Allen and Seyfried, 2004).

It was recently demonstrated (Alt and Shanks, 2003; Sharp and Barnes, 2004) that serpentinization plays and important part in the balance of S and Cl in Hess crust–hydrosphere systems. Alt and Shanks (2003) have also demonstrated that serpentinization is accompanied by the depletion of seawater in S, and the temperature regime of this process controls the S isotopic composition of the serpentinite. The Cl balance during serpentinization was considered by Sharp and Barnes (2004), who presented data testifying that Cl is concentrated in peridotites in the course of their serpentinization within the temperature range of 25–230°C. Some Cl is thereby contained in the serpentinite in the form of an intergranular salt phase. According to (Sharp and Barnes, 2004), peridotite hydration into serpentinite produces a highly saline fluid, which can then precipitate dissolved chlorides. Their research led Sharp and Barnes to conclude that serpentinites in the Hess crust can serve as the main S conduit into the mantle and the principal agent in the transportation of Cl in its planetary geochemical cycle.

The most reliable geochemical indicator of the degree of serpentinization of mantle peridotites in slow-spreading ridges is the $^{87}Sr/^{86}Sr$ isotopic ratio, which can reach the values typical of seawater and even higher in whole-rock samples of almost completely serpentinized oceanic peridotites (Snow and Reisberg, 1995). According to the calculations in (Snow and Reisberg, 1995), the W/R ratio at which oceanic peridotites are serpentinized often exceeded 10000. The $^{87}Sr/^{86}Sr$ isotopic ratio in MAR serpentinites shows a positive correlation with the Sr, Ca, and U concentrations in these rocks, a fact indicating that these elements are introduced in ultramafic rocks during their serpentinization (Silantyev and Belyatsky, 1998).

Phase transitions in ultramafic rocks at the downwelling limb of a hydrothermal circulation cell were studied by means of numerical simulations (Silantyev et al., 1992; Grichuk, 2005). Considered together with available empirical data (see, for example, Bazylev, 2003), these results make it possible to draw a provisional *T* vs. W/R diagram of mineral assemblage related to the mineral transformations in MAR peridotites during their successive hydration.

Inasmuch as mantle peridotites are exposed over vast seafloor areas in the crest zones of slow-spreading ridges, the evolution of the chemical composition of these rocks during their serpentinization inevitably affects global geochemical cycles in the hydrosphere–oceanic (Hess-type) crust and crust–mantle systems. In the latter instance, it should be taken into account that the material of the oceanic crust displaced from MOR to subduction zones is one of the main sources of magmatism in the active ocean–continent transition zone, and its geodynamic type controls the geochemical specifics of the subduction magmatic complexes. Conceivably, the crust of the Penrose type (with a well pronounced basaltic layer) serves in subduction zones as a source of lithophile and strongly incompatible elements in the suprasubduction magmatic system, whereas the crust of the Hess type (peridotite) in subduction zones is a principal donor of water, siderophile, and some incompatible elements (first of all, Sr) (Silantyev and Belyatsky, 1998). Also, it cannot be ruled out that geodynamic conditions may occur beneath the crest zones of slow-spreading ridges that are favorable for the melting of residual peridotites, and this leads to the derivation of melts with subduction geochemical signatures. This idea was put forth for gabbroids at 37°N within MAR (DSDP Hole 334). The parental melts of these

rocks show geochemical features of andesite–boninite magmas (Nonnotte et al., 2005). The geochemical signatures of the recycled serpentinized Hess crust subducted deep into the mantle can be partly inherited by the deep sources of mantle magmatism whose melting gives rise to the parental melts of enriched MORB.

The above brief review of information on hydrothermal systems acting in peridotites at slow-spreading MOR led us to conclude that the least explored aspect of the problem discussed herein is the influence of the duration of interactions in the system peridotite–seawater-derived fluid on the mineralogical and chemical effects related to hydrothermal transformations in the Hess crust.

SIMULATION TECHNIQUES

Simulation of Chemical Interactions

Irreversible reactions of rock-forming minerals with seawater were simulated within the framework of a model that involved the description of the dissolution kinetics of minerals and the calculation of the equilibrium composition of the system at each time step. Our simulations were underlain by the following assumptions: (1) secondary phases are synthesized by passing through a stage of the dissolution of primary minerals; (2) the aqueous solution has an equilibrium chemical composition; and (3) the precipitation of secondary minerals is controlled by their solubility and is a much faster process than dissolution (Helgeson, 1968). Hence, at any time step, the mineral association consists of incompletely dissolved primary minerals, previously formed secondary phases, and newly precipitated minerals that are in equilibrium with the aqueous solution.

Chemical interactions are simulated as a set of successive equilibria occurring at each time step. The chemical balance of the system is thereby simulated based on the chemical balance of the aqueous solution at the previous step and the current dissolution rates of the minerals. The molar amount x_i of mineral i dissolved at each step is calculated as $x_i = Fs_i S_i r_i \Delta t$, where S_i is the surface area of mineral i, r is the instantaneous dissolution rate of the mineral (mol cm^{-2} s^{-1}), and Δt is the duration of the time step (s). Minerals precipitated during previous steps are regarded as primary and can be dissolved if they are not in equilibrium with the solution of current composition. The duration of each step is calculated automatically by constraining the introduction of the mass of the most quickly dissolving mineral. The surface area of primary minerals in the pristine rock is calculated from the specified sizes of mineral grains and the mineralogical composition of the rock. The term Fs ($0 < Fs_i < 1$) controls the acceptability of the surface of a mineral to the aqueous solution. It can be interpreted in terms of rock disintegration, its minute fracturing, effective porosity, etc. The surface area of primary minerals is continuously recalculated at each time step with regard for the decrease in the grain size due to their dissolution. The surface area of secondary minerals is calculated from the specified grain sizes and the mass of the newly formed minerals.

Dissolution Kinetics of Minerals

The dissolution rate of minerals at each time step is calculated for the instantaneous pH value and the deviation from equilibrium between a mineral and solution by the formula

$$r_i = [k_{0H^+}(a_{H^+})^{b(T-T_0)+n_0} + k_{0H_2O} + k_{0OH^-}(K_W a_{H^+})^m] \times \exp\left[\frac{E_a}{R}\left(\frac{1}{T_0} - \frac{1}{T}\right)\right] \times k\left\{1 - \exp\left[p\left(\frac{\Delta G}{RT}\right)^q\right]\right\}.$$

In this equation, the first term in brackets describes the dependence of the dissolution rate on the pH of the solution (Kump et al., 2000; Brantley, 2004) at T_0 = 298.15 K (this is the conventional formalism for representing experimental data on the dissolution kinetics of minerals). The two former terms compose a sort of the Arrhenius equation that describes the temperature dependence of the dissolution rate of a mineral at activation energy E_a. The last term describes the deceleration of the dissolution rate of the mineral when equilibrium is approached (Lasaga, 1981; Aagaard and Helgeson, 1982; Brantley, 2004); the parameters k, p, and q are equal to 1 for most minerals. The approach applied herein in order to model the dissolution kinetics of minerals was described in detail in (Zolotov and Mironenko, 2007).

The following data were used for olivine: E_a for forsterite was compiled from (Wogelius and Walther, 1992); we interpolated k_{0H^+} and n_0 for Ol_{93} from data on forsterite from (Chen and Brantley, 2000) and fayalite from (Wogelius and Walther, 1992), K_{0H_2O} from (Pokrovsky and Schott, 2000). Data on pyroxenes (for pH < 6) and serpentine were borrowed from (Brantley, 2004). Data on Fe oxides and hydroxides, amphiboles, spinel (for which the parameters of corundum were used), and brucite (imitated by gibbsite) were taken from (Alekseev, 2005). The E_a of magnetite was from (Sidhu et al., 1981), and K_{0H_2O} and n_0 are from (Alekseev, 2005) for the incongruent dissolution of magnetite. For saponites (imitated by montmorillonite) and chlorites, we used data from (Alekseev, 2007); the data for pyrite and pyrrhotite are from (Thomas et al., 2000). For talc we assumed kinetic constants for tremolite recalculated to 1 f.u. The kinetic constants of dissolved carbonates were evaluated from data in (Dobrovol'skii, 1978).

Thermodynamic Calculations

The thermodynamic unit of the model is based on the GEOCHEQ complex (Mironenko et al., 2000), which enables calculating equilibrium in systems with aqueous solutions, minerals, and gases. The thermodynamic properties of aqueous species in the database are compiled mostly from (Shock et al., 1989, 1997), data on minerals are mostly from (Helgeson et al., 1978; Holland and Powell, 1998), thermodynamic properties of montmorillonite, illite, baddeleyite, and saponite are from (Vieillard et al., 2004; Wilson et al., 2006; Wolery and Jove-Colon, 2004). The thermodynamic data make it possible to simulate equilibria within the temperature range of 0–500°C and pressures of 1–5000 bar. The simulations were made in the system O–H–Si–Al–Mg–Fe–Ca–Na–Cl–S–C.

Input Data and Model Description

The physicochemical simulation of transformations in the crust of slow-spreading ridges relies onto available data on the inner structure of various geological vertical sections, the mineralogy of the rocks, variations in the *P–T* parameters with depth down the sections, and current concepts concerning the hydrodynamics of a hydrothermal cell. The adequacy and plausibility of the model were estimated based on similarities between the simulated spatiotemporal variations in the mineral transformations and the secondary mineral assemblages of the rocks.

Structure of the Hess Crust

Already early in the course of our research (Silantyev et al., 1992), we proceeded from the then-existing concepts concerning the Hess crust structure. Since then these concepts were remarkably specified and appended based on results obtained in the course of deep-sea drilling during ODP legs 118 and 209 (Dick et al., 1991; *Shipboard…*, 2003) and IODP expeditions 304 and 305 (Blackman et al., 2002) and by dredging at 3°–12°E at the Gakkel Ridge during the AMORE 2001 expediion (Michael et al., 2003), at 13°–15°N at MAR during the Serpentine 2007 expedition (*Shipboard…*, 2007), as well as observations aboard submersibles (Kelley et al., 2001; Silantyev et al., 2007). Data obtained over the past decade suggest that the central portions of amagmatic segments of slow- and ultraslow-spreading ridges are made up of large gabbroid massifs locally overlain by thin sheets of pillow lavas and, in the marginal parts, serpentinized peridotites (Dick et al., 2003, 2006). It was also established that large (up to 200 km^2) exposures of mantle peridotites compose not only inner-corner highs in slow-spreading ridges but also the walls of their rift valleys (Silantyev et al., 1991; Cannat et al., 1997; Karson, 1998).

Because of this, our simulations were carried out for a simplified vertical crustal section of a slow-spreading ridge of the Hess type that consists only of mantle peridotites (spinel harzburgites) (Fig. 1). The inner structure of this sections is close to naturally occurring vertical sections of slow- and ultraslow-spreading ridges (MAR and the Gakkel Ridge). The simulations were made with the compositions of natural rock-forming minerals: olivine, orthopyroxene, clinopyroxene, and spinel from a typical harzburgite from MAR. The size of the spinel and accessory pyrrhotite grains was assumed to be 0.1 mm, and those of grains of all other minerals were taken up to be 1.0, which roughly corresponds to the actual granulometric relations in the rocks. The grains of the secondary minerals were taken to be 0.005 mm. The coefficient *Fs* was assumed to be 0.0005.

Hypothetical Hydrodynamics of the System

The assumed input parameters of the model oceanic hydrothermal system were as follows. The hydrothermal system has the shape of an inverted cone with the apex at the MAX axis at a depth of 11.25 km (the thickness of the oceanic crust). The active water catchment area at the ocean's surface is 100 km^2 (*Report…*, 2004). The effective porosity of the rock was assumed to be 10%. The annual average discharge of solution in the hydrothermal convective cell is 4.73×10^6 t/year [it was calculated from data presented in (Grichuk, 2000)]. This seawater flow percolates downward through the hyperbasites, gradually focuses at the ridge axis, and is then discharged at the seafloor surface in the form of an upwelling flow ascending from a depth of 11.25 km. The pressure at the seafloor surface is equal to the hydrostatic pressure of the seawater column and increases with increasing lithostatic pressure of the rocks ($\rho = 3.2$) with depth. The temperature at the seafloor surface is 4°C and increases corresponding to the geothermal gradient in the axial part of MAR (Sleep, 1978).

The model system is schematically represented in Fig. 2. The integral volume of the crustal block involved in the hydrothermal process is subdivided into 22 individual blocks. We assumed that a solution portion (initially it is seawater) entering block *j* resides within it for a time period Δt_j, during which chemical interactions occur, and then the modified solution inflows into the underlying rock block having other *T* and *P* parameters, whereas block *j*, which has undergone mineral transformations, receives a new portion of the solution. We simulated the passage of ten solution waves. The residence time Δt_j of solution in the block was calculated from the assumed values of the hydrothermal system debit and the volume of the rock block. Because the area of horizontal sections of the block decreases with depth, the percolation velocity progressively increases from 0.5 m/year for the uppermost block to 900 m/year for the lowermost one, and the residence time of solution in a block correspondingly decreases. The initial mass ratio of the solution and

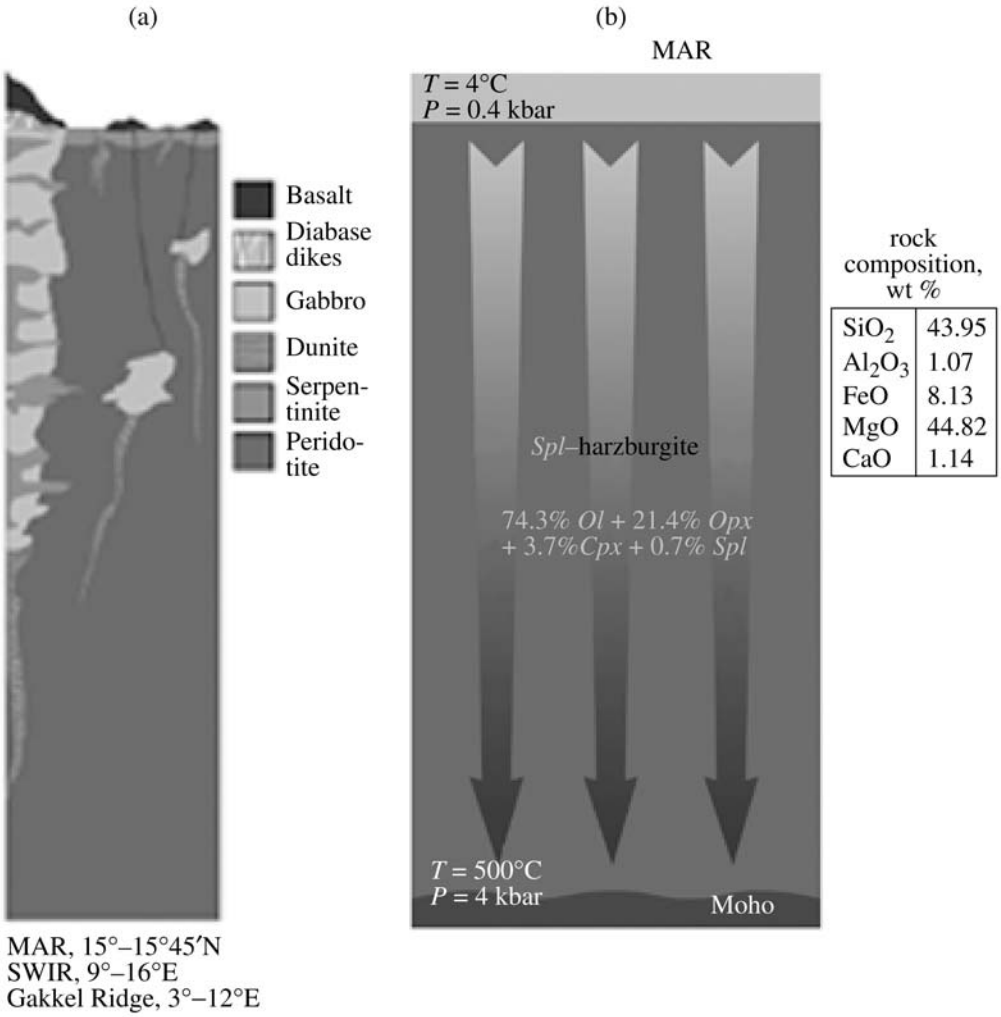

Fig. 1. Generalized schematic representation of the vertical section of Hess crust at a slow-spreading ridge (Dick et al., 2003), the Southwest Indian Ridge (SWIR), and (b) the inner structure and composition of the original model vertical section of the oceanic crust assumed in our research.

rock (W/R) in the block was taken to be 1 (water loss to hydration was ignored).

A significant disadvantage of this model was the inconsistency between its kinetic–thermodynamic unit, in which small and optimal time steps are used, and the oversimplified concept of the hydrodynamics of the system, in which the flows of large enough solution portions from block to block are separated by significant time intervals.

RESULTS OBTAINED BY SIMULATING PHASE EQUILIBRIA AND MATERIAL BALANCE IN HYDROTHERMAL SYSTEMS THAT CIRCULATE IN PERIDOTITES WITHIN SLOW-SPREADING RIDGES

Below we describe various newly formed minerals simulated for discrete blocks in the downwelling limb of the hydrothermal cell. The extent of development of these mineral assemblages and the degree of hydrothermal transformations in the pristine rock are not described in much detail, although all this information was provided by our simulation results. It should be mentioned that the mass of newly formed minerals notably increases with depth as the temperature increases, as also do the dissolution rates of minerals.

Phase Transformations in the Peridotites

Figure 3 schematically represents the succession of minerals newly formed when hydrothermal fluid percolates through spinel harzburgite in the model cross section. This situation is reached 1000 years after the onset of hydrothermal interaction in each block. One of the first products of hydrothermal transformations in peridotites is goethite, which is formed at temperatures as low as $T = 19°C$ and indicates that peridotite is oxidized by seawater. At a temperature of 63°C, which corresponds, according to the assumed parameters (Table 1),

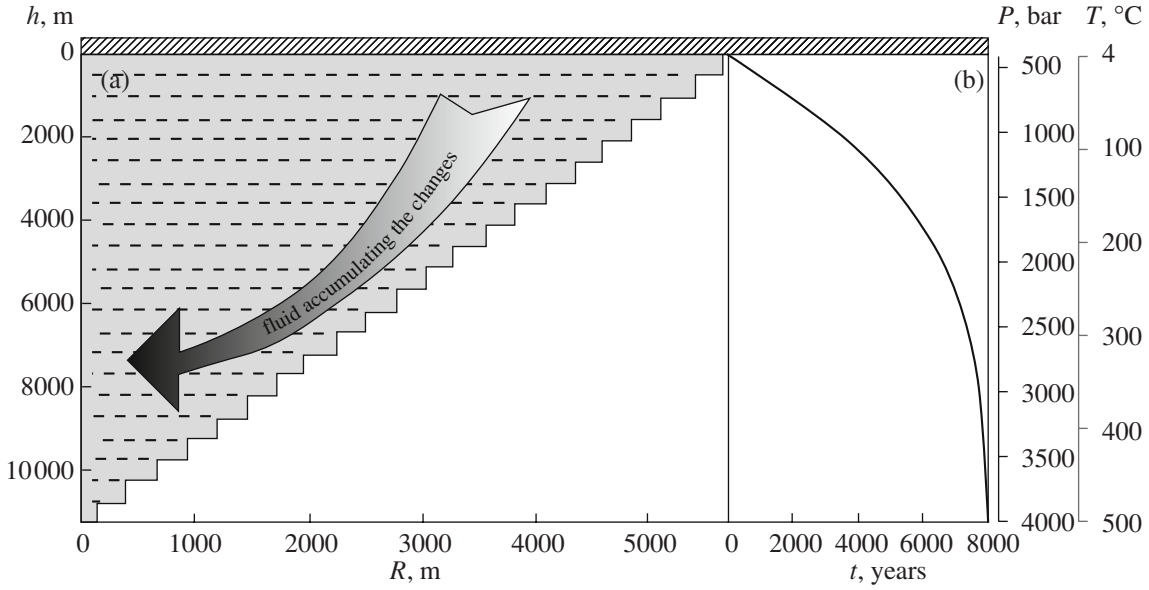

Fig. 2. Model representation of the downwelling limb of the system peridotite–hydrothermal solution.
(a) Cross section of a cone-shaped hydrothermal reactor within the depth range of the crustal vertical section, *R* is the distance from the ridge axis; (b) variations in the interaction time of the host peridotite and hydrothermal fluid depending on the depth level (temperature and pressure).

to a depth of approximately 1500 m in the vertical section, goethite gives way to hematite. Pyrite first appears also in the low-temperature (19°C) and shallow-depth part of the section. The association of pyrite and hematite persists in the section up to a temperature of 107°C. The temperature range of 107–129°C is marked by the decomposition of pyrite and hematite and their replacement by the pyrrhotite–magnetite association. When the same wave of hydrothermal fluid interacts with deeper parts of the vertical section, magnetite and pyrrhotite remain stable to a depth of 11 km ($T = 482$°C).

At low-temperature transformations of peridotite near the surface (19°C, 511 m), aragonite is synthesized, which gives way to dolomite at greater depths (41°C, 1022 m). Obviously, this crystallization succession of carbonates reflects the compositional evolution of the hydrothermal fluid (see below). Considering the results of our simulations (Silantyev et al., 2005) for the same peridotite–seawater model system with regard for the synthesis of solid solutions (including the aragonite–strontianite one), it can be added that aragonite is progressively depleted in the strontianite end member down the vertical section (with increasing depth). Silantyev et al. (2005) have demonstrated that the successive addition of seawater-derived fluid to the model system (i.e., with an increase in the W/R ratio) results in the expansion of the aragonite stability field to a temperature of about 100°C.

Judging from our simulation results, chlorite remains stable throughout the whole temperature range in question (i.e., from 19 to 482°C). In the lowest temperature region, this mineral is magnesian (clinochlore), and Fe-richer chlorite (daphnite) appears in the system only at a temperature of 239°C. The greatest chlorite content in the rock was noted within the temperature range of 239–261°C (i.e., at depths of approximately 5000–6000 m). It is important to emphasize that simulations with the use of data on chlorite solid solutions (clinochlore–daphnite; Silantyev et al., 2005) confirm the experimental data (Mottl, 1983) that the Fe mole fraction of Fe–Mg silicates (chlorite and amphibole) increases in a hydrothermal system with increasing

Table 1. Mineral associations simulated for hydrothermally altered harzburgite

Mineral association	*T*, °C	*P*, kbar	pH of solution
(I) *Arg* + *Gt* + *Sap*	19–63	480–810	8.25
(II) *Ctl* + *Hem* + *Py*	63–129	810–1300	8.50
(III) *Ctl* + *Mag* + *Po*	129–261	1300–2280	8.80
(IV) *Atg* + *Tr* + *Mag* + *Po*	261–416	2280–3430	6.15
(V) *Tlc* + *Tr* + *Ol* + *Mag* + *Po*	416–482	3430–3920	5.05

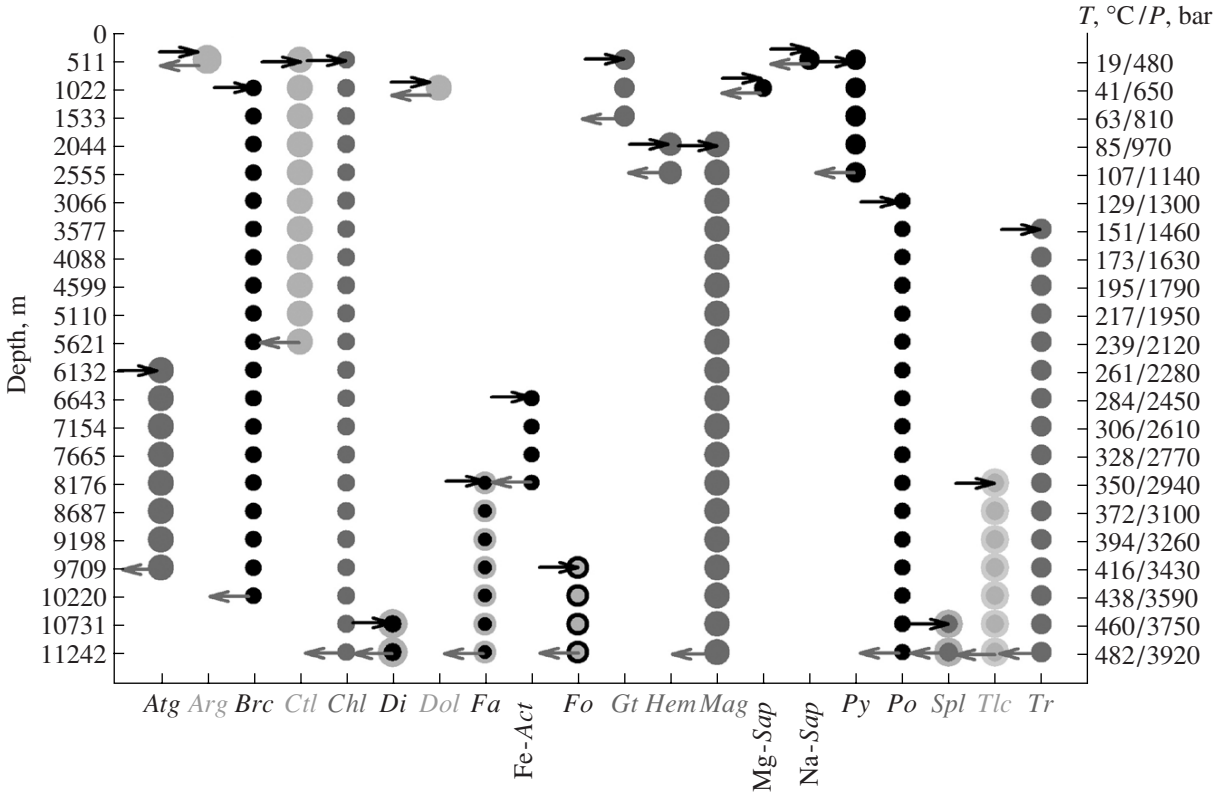

Fig. 3. Phase transformations in the model peridotite during its interaction with hydrothermal fluid 1000 years after the beginning of hydrothermal circulation.

temperature and decreasing W/R ratio. In the low-temperature (oxidized) zone of the model system, goethite appears almost simultaneously with Na-saponite, which is replaced by Mg-saponite with depth (T = 41°C). The stability field of saponite in hydrothermally modified peridotite is constrained by a temperature of 63°C (as also is the field of goethite). Brucite is synthesized in the model system at 41°C and persists in the rock to a temperature of 350°C. Serpentine (chrysotile) is synthesized in peridotite in insignificant amounts early in the course of the hydrothermal process (at T = 41°C). Further transformations of the ultramafic rocks are associated with a drastic increase in the degree of its serpentinization starting at a temperature of 107°C (see below). At a temperature of 261°C, chrysotile is replaced by aragonite, which remains stable in the model system to a temperature of 416°C. The very first traces of calcic amphibole (actinolite–tremolite) are discernible in the model system already at a temperature of 151°C. As the depth increases, this phase systematically appears in the following assemblages: chlorite + chrysotile + magnetite + pyrrhotite (151–239°C), chlorite + antigorite + magnetite + pyrrhotite (261–328°C), talc + chlorite + antigorite + magnetite + pyrrhotite (350–416°C), talc + chlorite + olivine + magnetite + pyrrhotite (416–460°C), and talc + chlorite + olivine + diopside + magnetite + pyrrhotite (460–482°C).

Talc appears in the system at 350°C and persists to higher temperatures. In the intermediate- to high-pressure segment of the downwelling limb of the hydrothermal cell, ferrous olivine is synthesized in the rock, and the Mg mole fraction increases with increasing temperature. Diopside occurs in equilibrium with solution at depth corresponding to a temperature of approximately ~460°C.

The results of our simulations allowed us to distinguish the following mineralogical facies of peridotite transformations at slow-spreading MOR within broad temperature and pressure ranges (Table 1, Fig. 4): (1) aragonite–goethite–saponite (Fig. 4, I), (2) chrysotile–hematite–pyrite (Fig. 4, II), (3) chrysotile–magnetite–pyrrhotite (Fig. 4, III), (4) antigorite–tremolite–magnetite–pyrrhotite (Fig. 4, IV), and talc–tremolite–olivine–magnetite–pyrrhotite (Fig. 4, V). Silanyev et al. (2005) proposed a qualitative scheme for the evolution of the fluid regime at various depth levels of the downwelling limb of a hydrothermal system in peridotite. According to this scheme, the mineral assemblages obtained within the scope of our model correspond to the following types of fluid regime typical of the crust of slow-spreading ridges: (I) zone of strongly oxidized conditions (fluid-dominated regime), (II) zone of moderately oxidized conditions, and (III–IV) zone of reduced conditions (rock-dominated regime).

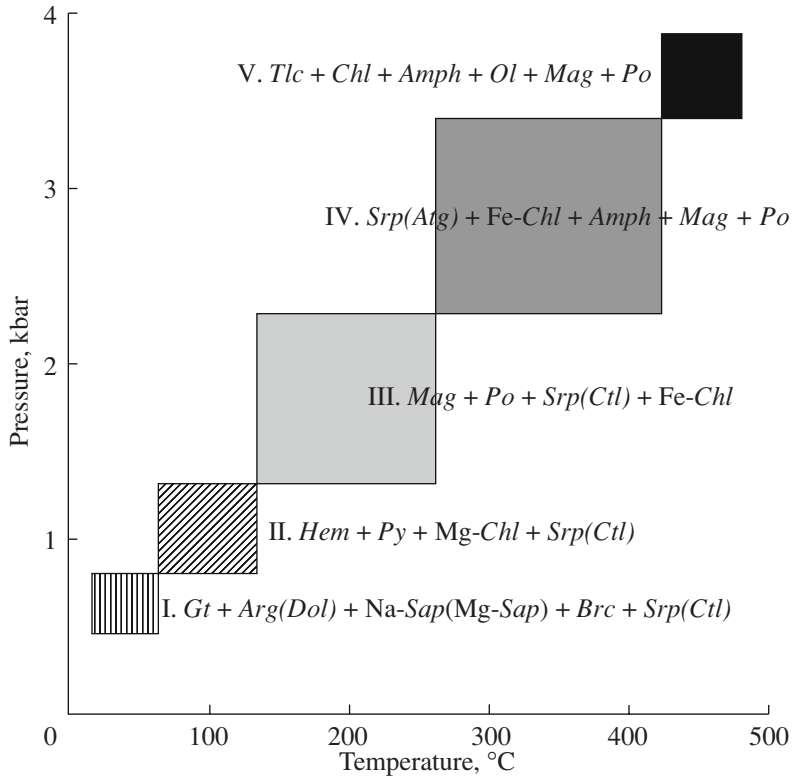

Fig. 4. Succession of minerals synthesized in the downwelling limb of the hydrothermal system in peridotite. (I) zone of strongly oxidized conditions; (II) zone of mildly oxidized conditions; (III–V) zones of reduced conditions.

Model simulations permitted us to provisionally propose the following replacement succession of primary minerals in model spinel harzburgite. Primary olivine starts to disappear from the rock in a very insignificant amount at temperatures as low as 85°C, after the passage of 3000 years of rock interaction with hydrothermal solution. The fast consumption of primary olivine corresponds to the temperature range of 151–328°C, and the mineral completely disappears from the rock at a temperature of 328°C. The content of primary orthopyroxene in the rock begins to insignificantly decrease starting at a temperature of 195°C (after 8000 years of hydrothermal interaction), this mineral is most actively decomposed in the rocks starting at 328°C, and its content reaches a minimum at a temperature of 438°C. According to the results of our simulations, primary clinopyroxene is less stable than orthopyroxene in hydrothermal environments and starts dissolving at a temperature as low as 107°C. The active consumption of clinopyroxene in the rock begins after the passage of 6000 years of interaction with hydrothermal fluid, at a temperature of 151°C. The behavior of primary spinel in the model hydrothermal system is evidently controlled by variations in the pH of the fluid, and the content of this mineral in the rock can drastically decrease with a significant decrease in pH. The primary ore phase in the model system is pyrrhotite. As follows from our simulations, this mineral starts to actively dissolve 4500 years after the onset of fluid circulation, at a temperature as low as 41°C.

One of the tasks of our simulations was to evaluate the time required for the effective serpentinization of ultramafic rocks at slow-spreading MOR under various *P–T* conditions. Note that these estimates are merely provisional at the current state of the simulations and may involve significant inaccuracies. The analysis of the effect of various factors on the dissolution rates of minerals indicates that the possible errors depend not so much on the inaccuracies in the kinetic parameters of the dissolution of minerals as on the assumptions concerning the surface areas of minerals in contact with solution. In this situation, it is more reasonable to discuss the relative intensity of hydrothermal transformations in the rocks at various depth levels and various temperatures. Our simulation results demonstrate that the degree of peridotite serpentinization (SD = serpentine/rock, %) at low-temperature interaction with seawater, when the rock is exposed at the seafloor surface, is extremely low (SD = 0.11) even after the passage of 10000 years. Serpentinization becomes effective (SD ~ 70) at temperatures of approximately 130–150°C, after ~4800 years of interaction with hydrothermal fluid (Fig. 5). Our data suggest that most serpentinites in slow-spreading ridges (usually SD ≥ 60) were produced at temperatures of no lower than 130°C, i.e., at depths of 3.5–4.5 km within the crustal section.

Table 2. Temperature, pH, and concentrations of dissolved gases simulated for model hydrothermal fluid and obtained empirically in (Tivey, 2007) for hydrothermal vents at the Rainbow and Lost City hydrothermal fields

Mineral association	*T*, °C/*P*, bar	pH	H_2, mol/kg of H_2O	CH_4, mol/kg of H_2O	ΣH_2S, mol/kg of H_2O	ΣSO_4^{2-}, mol/kg of H_2O
Simulated by our model						
Arg + *Gt* + *Sap*	20–60/ 480–810	8.25	1.7×10^{-10}	1.1×10^{-15}	2.3×10^{-7}	1.7×10^{-2}
Ctl + *Hem* + *Py*	61–130/ 810–1300	8.50	1.6×10^{-2}	1.8×10^{-5}	3.7×10^{-04}	3.8×10^{-3}
Ctl + *Mag* + *Po*	131–260/ 1300–2280	8.80	7.1×10^{-2}	2.7×10^{-5}	4.9×10^{-3}	2.9×10^{-18}
Atg + *Tr* + *Mag* + + *Po*	261–420/ 2280–3430	6.15	1.74	4.5×10^{-5}	6.3×10^{-3}	1.9×10^{-20}
Tlc + *Tr* + *Ol* + + *Mag* + *Po*	421–480/ 3430–3920	5.05	2.24	5.2×10^{-5}	1.0×10^{-2}	7.9×10^{-19}
Rainbow hydrothermal field						
Srp + *Arg* + *Chl* (*Gross* + *Di*)	365 –	2.8 (at 25°C)	1.3×10^{-3}	1×10^{-3}	1.3×10^{-4}–2.2×10^{-3}	0
Lost City hydrothermal field						
Srp + *Arg* + *Brc* (*Ta* + *Amph*)	≤91 –	10–11 (at 25°C)	$<1 \times 10^{-3}$–1.5×10^{-4}	$<6.4 \times 10^{-5}$	1×10^{-3}–2×10^{-3}	1×10^{-3}–4×10^{-3}

Systematic Variations in the Whole-Rock Composition of the Peridotite

The simulation results demonstrate that the bulk-rock composition of peridotites is most significantly modified near the surface (at temperatures of 19–41°C), mostly in the form of Ca introduction and Mg removal (Fig. 6). This depth level in the downwelling limb of the hydrothermal system is also characterized by the weak introduction of FeO and SiO_2 into the rock (Fig. 6). At higher temperatures and pressures, the whole-rock composition of the model peridotite does not display any significant transformations.

Systematic Variations in the Composition of the Hydrothermal Fluid

Figure 7 and Table 2 demonstrate the main tendencies in the variations in the concentrations of gases in the hydrothermal fluid and their correlations with the evolution of the redox conditions in the model system.

The hydrothermal transformations of peridotites near the surface in the upper part of the vertical section) brings about a zone of the adaptation of the hydrothermal solution, which is characterized by the most contrasting compositional transformations in the water–rock system. The material balance and phase transition in the narrow temperature range in this zone are controlled mostly by the absence of equilibrium between the peridotite and seawater, which acts as an oxidizer. In this zone, seawater interacting with peridotite is enriched in H_2, H_2S, CH_4, CO and depleted in CO_3^{2-} and SO_4^{2-} (in spite of the sluggishness of the corresponding reactions). The consumption of the carbonate and sulfate ions is reflected in the synthesis of aragonite, dolomite, and pyrite. Within the temperature range of 19–129°C, the pH of the solution slightly increases. Our simulations also demonstrate that CH_4 is effectively generated starting at a temperature of approximately 130°C at a depth of 3 km in the vertical section (the zone of effective serpentinization) and continues until CO_3^{2-} is completely consumed in the seawater-derived fluid. The H_2 concentration in the fluid continuously increases due to the oxidation of Fe^{2+} in primary olivine and pyroxenes under the effect of water, with the precipitation of magnetite. Inasmuch as water at deep levels of the section is actively spent on the hydration of the rocks, the concentrations of reduced gases in the fluid drastically increases. The monotonous increase in the H_2S concentration in the fluid at intermediate and deep levels of the downwelling limb of the cell is controlled by the solubility of primary pyrrhotite. Hence, a decrease in the redox potential in the system during the percolation of seawater-derived fluid into the oceanic crust is clearly pronounced in an increase in the $\sum CH_4/\sum CO_2$ and $\sum H_2S/\sum SO_4^{2-}$ ratios. As follows from our simulation results (Table 2), the hydrothermal fluid practically completely loses its SO_4^{2-} in the transitional zone from the oxidized to reduced regime, whereas pyrite is replaced by pyrrhotite and hematite is replaced by magnetite. The pH of solution in the high-temperature part of the system (261–482°C)

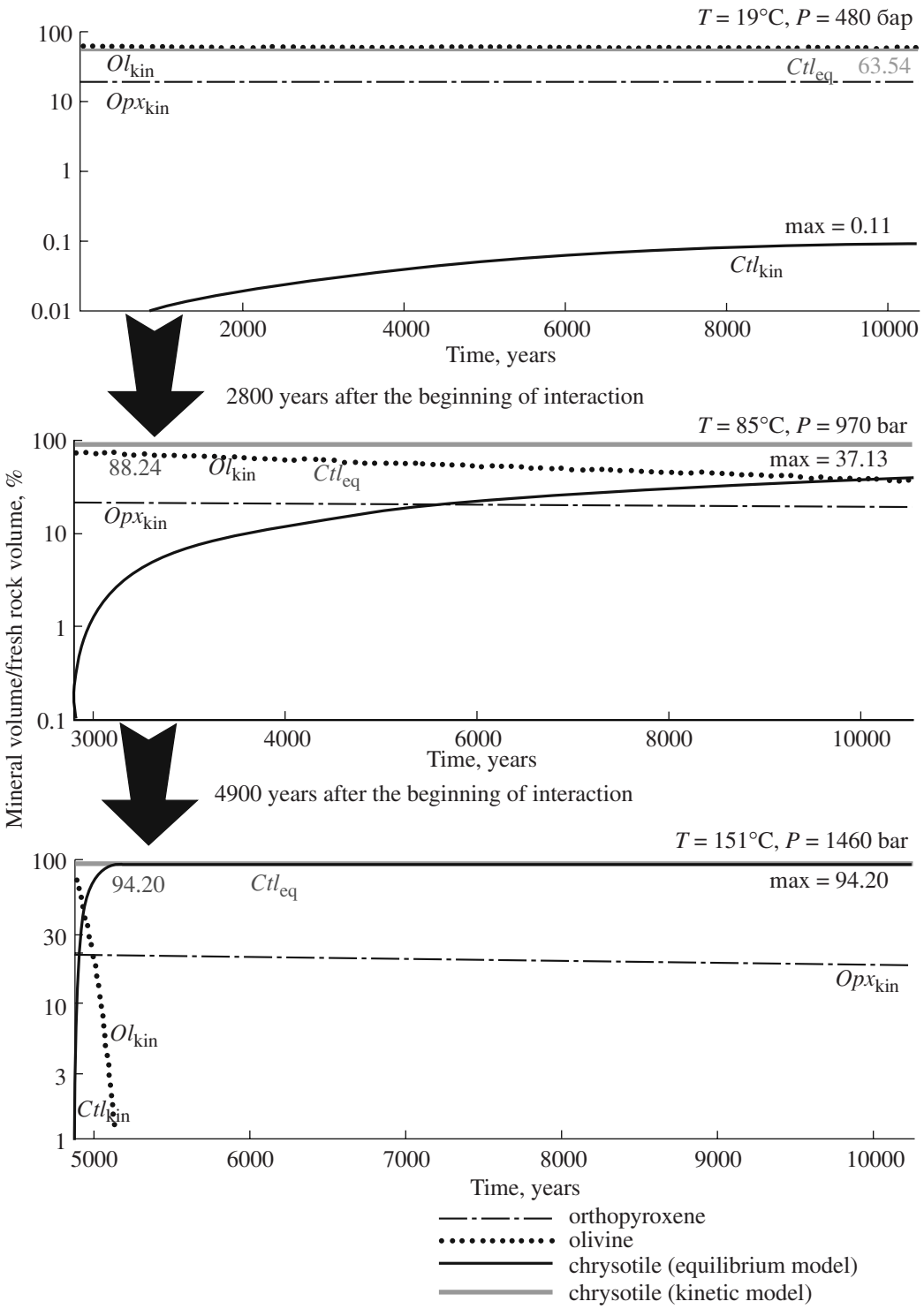

Fig. 5. Dissolution intensity of primary olivine and orthopyroxene in model peridotite and the effectiveness of serpentine formation evaluated according to the kinetic (kin) and equilibrium (eq) models for the model system at various depth levels in the vertical section.

systematically decreases to approximately 5. The solutions in our model vertical sections to a depth of approximately 7000 m generally remains weakly alkaline.

In the course of its percolation through ultramafic rocks, the hydrothermal solution becomes more and more strongly mineralized, because water is spent on the hydration at the inert behavior of chloride. A tem-

perature increase is also associated with an increase in the concentrations of Si, Fe, and Na in the solution.

VERIFICATION OF THE MODEL AND ITS GEODYNAMIC APPLICATION

Our simulation results can be applied in the reconstructions of geodynamic conditions favorable for the development of hydrothermal systems related to serpentinites in slow-spreading ridges. In this context it seems to be expedient to compare our simulation data on phase transitions in hydrothermally modified peridotites and on the compositional evolution of the hydrothermal fluid with available empirical data on natural hydrothermal systems in slow-spreading ridges. For the purposes of this comparison, we selected the thoroughly examined Rainbow and Lost City hydrothermal fields in MAR segments with the Hess crust.

The *Rainbow hydrothermal field* is located within the MAR rift valley (36°14′N, 33°53′W), in completely serpentinized peridotites in the lower part of the rainbow Ridge, which was produced by nontransform faulting in the axial MAR zone. In the west (near the wall of the rift valley), the Rainbow hydrothermal field is limited by a steep meridional fault. The exposed peridotites host sulfide stockworks. Pillow lavas were detected only east of the hydrothermal field and at the top of the Rainbow Ridge and, thus, overly the serpentinites, although no contact between the serpentinites and basalts was found (Fouquet et al., 1998). The Rainbow hydrothermal field is characterized by the highest temperature (365°C) among those measured at MAR hydrothermal systems, high concentrations of chloride (750 mM), metals (Fe, Cu, Zn, Co, and Ni), REE, K, Rb, and Cs at extremely low pH values (2.8) (Douville et al., 2002). The composition and temperature of hydrothermal vents at the Rainbow field are thought to provide evidence of the phase separation of the hydrothermal fluid in the root part of the circulation system (Fouquet et al., 1997). Strongly modified serpentinites in this area mineralogically resemble rodingites. These rocks consist of serpentine, aragonite, chlorite, rare grossular, and large grains of secondary diopside (Marques et al., 2006). According to (Marques et al., 2006), such a mineral assemblage could be produced in peridotites during Ca mobilization in the course of the retrograde serpentinization of the host rocks.

The *Lost City hydrothermal field* is situated on an tilted terrace in the upper part of the southern (near the fault) slope of the Atlantis Massif. This massif is restricted to the intersection of an offset of the Atlantis transform fault and MAR at 30°N and is made up of a rock association typical of the plutonic complex of slow-spreading ridges: peridotites, gabbro, and subordinate amounts of diabase and trondhjemite dikes and veins. The whole upper part of the near-fault slope of the Atlantis Massif consists of mantle peridotites that are now transformed into variously deformed serpentinites replacing harzburgites. A strongly subordinate

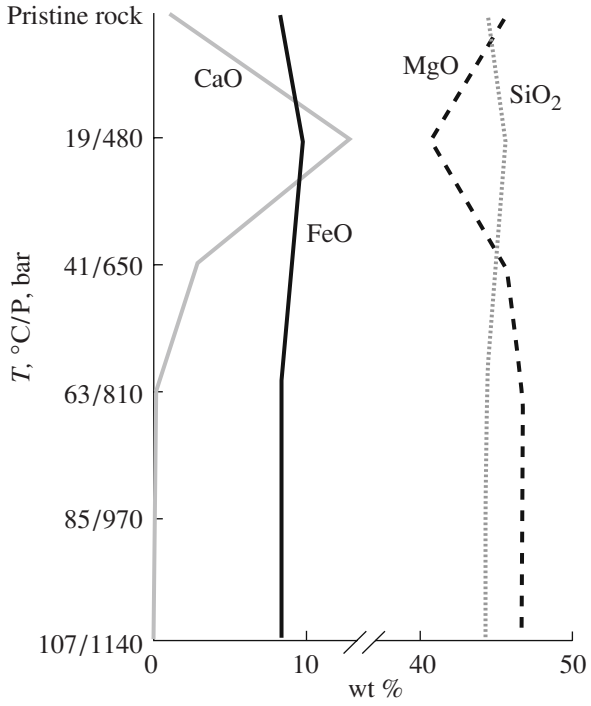

Fig. 6. Systematic variations in the bulk-rock composition of model peridotite during its low-temperature hydrothermal transformations.

role in the southern slope of the Atlantis Massif is played by metamorphosed gabbroids. The "peridotite core" of the Atlantis Massif (so-called *oceanic core complex*) contains abundant mylonitized rocks that mark zones along which some slabs of serpentinite slipped relative to one another. In addition to serpentinites, the upper part of the massif contains talc–amphibole schists, metagabbro, and minor amounts of acid vein rocks (*Expedition…*, 2006). Blackman et al. (2002) report data obtained during submarine observations aboard Alvin submersible, which testify that the upper part of the massif is intersected by a long-lived detachment fault along which the mantle material and lower crustal rocks were brought to the seafloor surface. Near the hydrothermal field, the serpentinites replacing harzburgites host relatively low carbonate chimneys and mats. The Lost City field itself includes tall carbonate spires composed mostly of Mg and Ca carbonate and brucite (the height of, for example, the Poseidon edifice is 60 m).

The Lost City hydrothermal field displays clearly pronounced physicochemical specifics that make it different from other hydrothermal fields at MAR. The temperature of the discharged solutions at the seafloor surface does not exceed at this field 40–90°C, and their pH reaches 9–11 (Kelley et al., 2005). Kelley et al. (2005) explain such a high pH value by the precipitation of a carbonate phase associated with the serpentinization of peridotites. Proskurowski et al. (2006) report a temperature estimate obtained for the carbon-

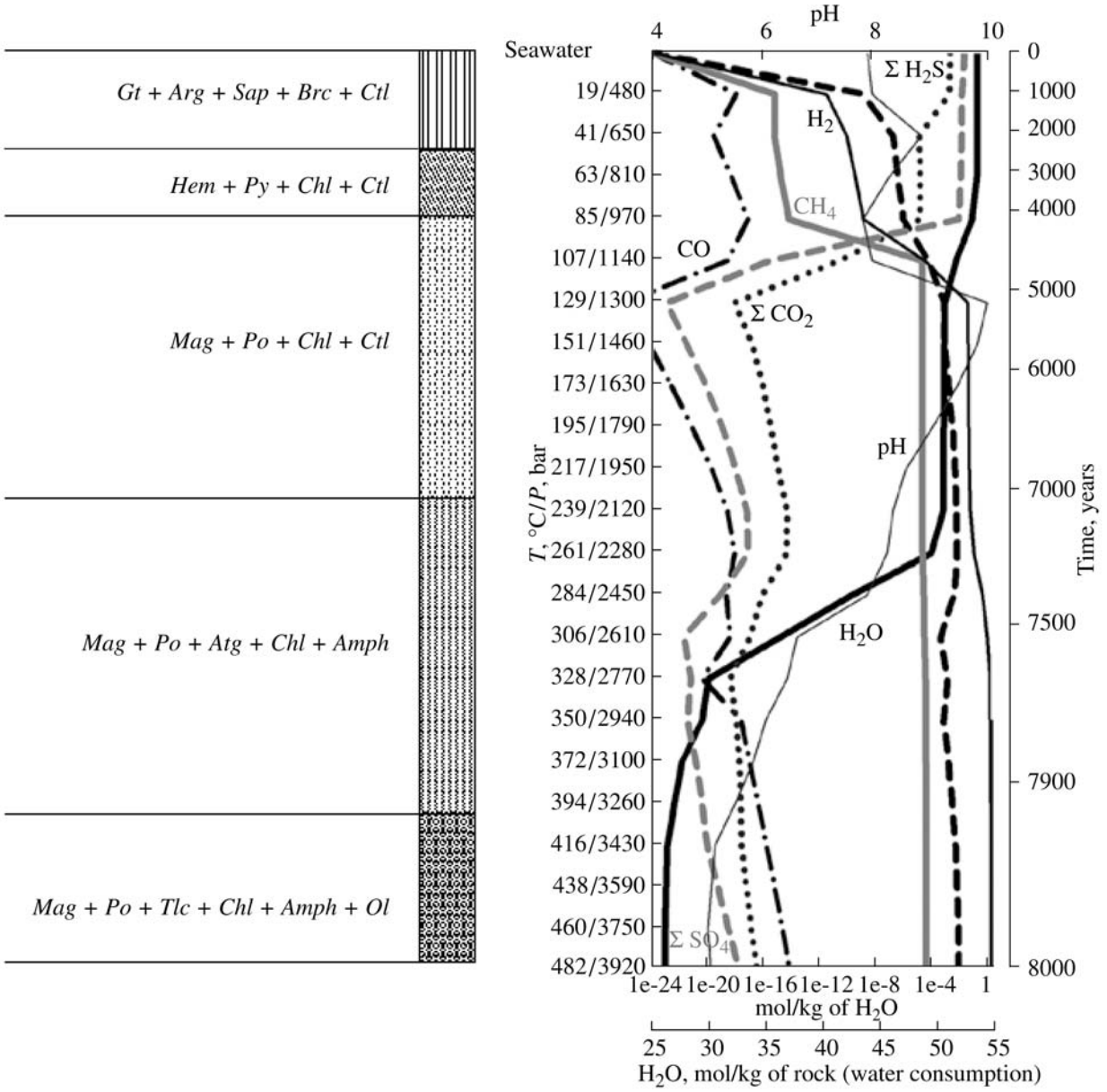

Fig. 7. Systematic variations in the concentrations of dissolved gases in hydrothermal fluid (second wave) and succession of mineral associations with depth in the model vertical section.

ate hydrothermal system at Lost City using the H_2O–H_2 and CH_4–H_2 isotopic thermometers. These estimates are 20–60°C higher than the measured values. According to Proskurowski et al. (2006), the possible reasons for this are as follows: (1) CH_4 and H_2 are generated at temperatures higher than 110°C, and (2) the isotopic equilibrium in the system at a temperature of 70°C is reached at the organogenic reduction of sulfates. The CH_4 concentration (55 nM) in the water column above the Lost City hydrothermal field is 30 times higher than the background concentration of this gas in seawater at the seafloor, and the H_2 concentration (349 nM) in the bottom water in the same area is >100 times higher than the corresponding background value (Blackman et al., 2002). Dubinina et al. (2007) employed isotopic–geochemical characteristics (δD, $\delta^{18}O$, $\delta^{13}C$, and $^{87}Sr/^{86}Sr$) of the hydrothermal solutions and those of the material of brucite–carbonate edifices at the Lost City hydrothermal field to demonstrate that the hydrothermal solutions at Lost City were derived in relation to the serpentinization of ultramafic rocks at temperatures above 200°C and low W/R ratios (<1). Dubinina et al. (2007) arrived at the conclusion that the Lost City fluid filtered through already-modified (hydrated) rocks of the Atlantis Massif and conductively cooled prior to arriving to discharge zones at the seafloor. Previously deposited carbonate material could be captured during this stage, at the partial dissolution of vein carbonates

in serpentinites at the upper zones of the Atlantis Massif and the carbonate cement of sedimentary breccias underlying the hydrothermal edifices (Dubinina et al., 2007). Judging from the data in (Fruh-Green et al., 2003), the low-temperature hydrothermal reactors of the Lost City hydrothermal field remain active for 30000 years (carbon isotopic dating).

Observations aboard Alvin and Mir submersibles indicate that the Atlantis Massif is broken into blocks by a series of faults oriented parallel to the Alvis transform fault. Obviously, fault-related fractures penetrating deeply into the rocks facilitate the passage of hydrothermal solutions and control the distribution of hydrothermal vents on the seafloor surface. Results of the comparative analysis of petrological and geochemical features of residual peridotites at various depths in the Atlantis Massif suggest that the southern slope is made up of geochemically distinct rocks (Silantyev et al., 2007). The geochemical heterogeneity of harzburgites in the Atlantis Massif was interpreted (Silantyev et al., 2007) as resulting from the mutual tectonic displacements of at least two large peridotite slabs. One of them (1254–760 m) consisted of ultramafic rocks intruded by gabbro, diabases, and trondhjemites; and the other (3500 m) was made up of peridotites alone.

Comparison of Our Simulation Results and Empirical Data

The comparison of the characteristic mineral assemblages simulated and the aforementioned data on the mineralogy of the serpentinites hosting the Rainbow and Lost City hydrothermal fields allowed us to provisionally constrain the conditions that controlled the mineralogy of ultramafic rocks at the fields. As was mentioned above, peridotites at the Rainbow hydrothermal field consist of serpentine, aragonite, chlorite, rare grossular, and secondary diopside (Marques et al., 2006). Following these researchers, it is reasonable to suggest that this mineral assemblage was produced in peridotites at the mobilization of Ca. However, a more plausible mechanism of Ca introduction into the peridotites seems to be their contact interaction with gabbroids (rodingitization) but not the retrograde serpentinization of the host rocks, as was proposed in (Marques et al., 2006). An independent argument in support of the rodingitization of the peridotites is provided by the very high temperature of fluid emanations at the Rainbow field, which testifies that active crustal magmatic chambers occur beneath the rift valley of this MAR segment. The serpentine + aragonite association, which is typical of the Rainbow hydrothermal field, suggests that these rocks were formed at a crustal depth of approximately 5 km and a temperature of no lower than 260°C.

Bastite serpentinites replacing harzburgites and hosting the Lost City hydrothermal field (these rocks were sampled in the course of dives of Mir submersible and Cruise 50 of the R/V *Akademik Mstislav Keldysh*) consist of antigorite (0.16–2.55 wt % Al_2O_3, 3.52–9.43 wt % FeO*), actinolite (2.00 wt % Al_2O_3), and carbonate, which occurs in the form of younger veins in the peridotites (authors' original data). According to our simulation data, the antigorite + actinolite association is stable in hydrothermally modified peridotites at temperatures of 261–416°C and pressures of 2.3–3.4 kbar, which implies that, similarly to peridotites at the Rainbow hydrothermal field, the serpentinization of ultramafic rocks at the Lost City field proceeded at lower levels of the crustal section. Talc–amphibole schists in the upper part of the Atlantis Massif seem to mark detachment surfaces in the peridotite massif, and their genesis was related to metamorphic events at these tectonic zones. The brucite + aragonite association in veins cutting across the peridotites and in hydrothermal spires corresponds to the low-temperature phase of serpentinite evolution at the Lost City hydrothermal field. According to (Kelley et al., 2005), these phases precipitate when warm fluid with high pH and a high Ca concentration mixes with seawater, which serves as a Mg and HCO_3^- donor. In our model, the aragonite + brucite association is stable in hydrothermal systems localized near the surface, at temperatures of 19–63°C. It should be mentioned that our simulation data indicate that brucite is also stable in serpentinites at MOR at higher temperatures (>60–100°C). In this temperature range, brucite occurs in association with chrysotile. Bazylev (2000) has demonstrated that the brucite + serpentine association is stable in MOR peridotites at a temperature of 200°C and a very low W/R ratio (0.006–5).

Andreani et al. (2007) presented a generalized phase diagram for mineral associations in the MSH system. The diagram is based on compiled data of long-term experimental, calculation, and empirical studies of the evolution of the mineral composition of peridotites in the course of their hydration over a broad temperature and pressure ranges. Figure 8 shows that the simulated mineralogical facies of modified MOR peridotites are in good agreement with the stability fields of secondary minerals in the MSH system.

The comparison of the simulated compositional evolution of hydrothermal fluid along the downwelling limb of the hydrothermal system from the near-surface to root levels of the peridotite vertical section makes it possible, first, to assay the plausibility of the simulations and, second, to identify the geodynamic factors controlling the composition of hydrothermal emanations at the Rainbow and Lost City fields (Table 2). The results obtained by comparing the simulation and empirical data for similar temperature ranges testify to the plausibility of the estimates for the hydrothermal fluid composition. Data of our model simulations suggest that differences in the compositional parameters of hydrothermal vents at the Rainbow and Lost City fields are predetermined by the different depths of the corresponding hydrothermal circulation systems. The downwelling limb of the hydrothermal system reaches deeper levels of the crustal section at the Rainbow than

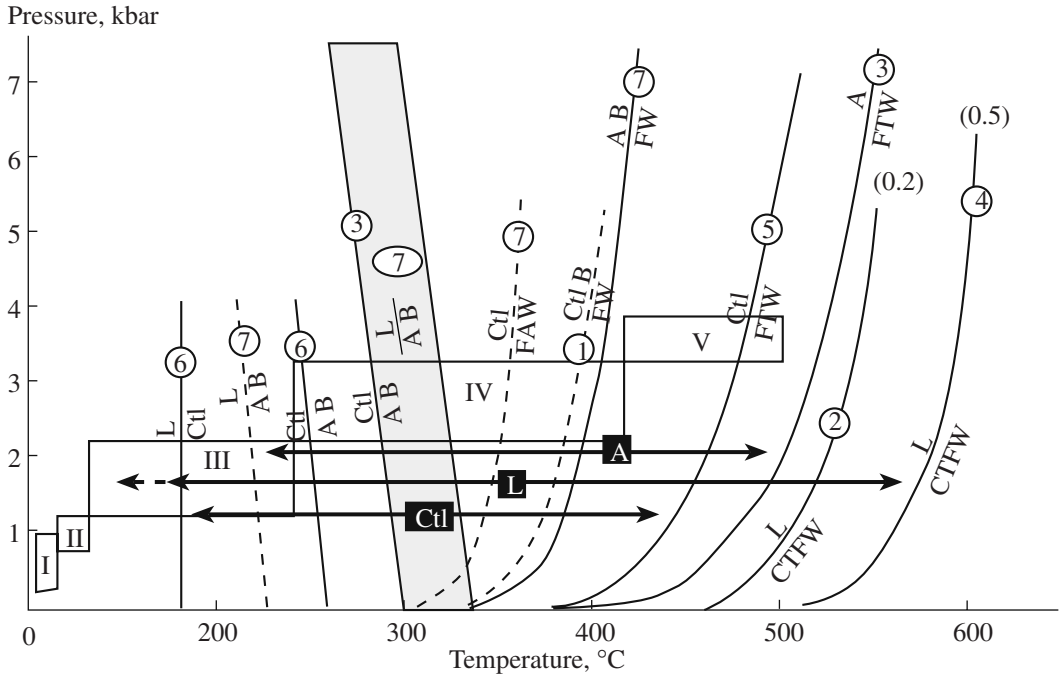

Fig. 8. Diagram of mineral assemblages formed during peridotite hydration (after Andreani et al., 2007).
Based on data from: (Johannes et al., 1968; Chernosky, 1973, 1988; Evans et al., 1976; Caruso and Chernosky, 1979; O'Hanley and Wicks, 1995; Evans, 2004). (0.2) and (0.5) are the Al concentrations in lizardite (f.u.), which corresponds to 3.7 and 9.2 wt % Al_2O_3. Phases: A—antigorite, B—brucite, C—chlorite, Ctl—crysotile, L—lizardite, F—forsterite, T—talc, W—H_2O. I, II, III, IV, and *V* are characteristic mineral assemblages of hydrothermally modified peridotites from our simulation model (see Fig. 4).

at the Lost City field, and this is responsible for the practically complete absence of SO_4^{2-} from the Rainbow hydrothermal emanations and the high Cl concentration in them (Mayanovic et al., 2007; Tivey, 2007). At the same time, the penetration of the downwelling limb of the Lost City hydrothermal system to shallower depths of the crustal section is confirmed by the fact that the hydrothermal emanations contain preserved SO_4^{2-}, whose concentration is comparable with the calculated one for temperatures of 61–130°C, and lower H_2 and H_2S concentrations.

Geodynamic Interpretation of Our Simulation Results

The data and materials presented above led us to propose the following geodynamic model for the development of the hydrothermal systems in peridotites at slow-spreading ridges:

(1) The serpentinization of mantle rocks at slow-spreading ridges takes place at crustal depths of 3.5–4.5 km.

(2) The major heat source of hydrothermal system in peridotites at slow-spreading ranges are gabbro intrusions.

(3) The serpentinites are exhumed to the seafloor surface, and this is associated with the development of large detachment faults.

(4) A combination of all of the aforementioned factors is a necessary condition to trigger the action of hydrothermal circulation systems in peridotites at slow-spreading MOR.

As was mentioned above, the results of our simulations imply that most serpentinites at slow-spreading MOR were formed at depths of about 3.5–4.5 km. Independent arguments in support of this conclusion are provided by data on the H, O, C, and Sr isotopic composition (Dubinina et al., 2007), which indicate that MOR ultramafic rocks are serpentinized at temperatures of > 200°C and a low fluid/rock ratio (<1). The deep-sitting (in the crustal section) nature of the serpentinization of mantle peridotites is clearly illustrated by the phase diagram of mineral assemblages in the MSH system (Fig. 8).

The close association of MOR peridotites with gabbroid intrusions was pointed out in many publications devoted to the compositional structure of inner corner highs consisting of peridotites cut by gabbro veins and dikes (for example, Silantyev et al., 1991; Cannat et al., 1997; Blackman et al., 2002). According to currently adopted concepts, gabbro intrusions is the major heat source in the cold lithosphere of slow-spreading MOR (see, for example, Baker et al., 2004; Allen and Sey-

fried, 2004). As was mentioned above, heat balance calculations (Allen and Seyfried, 2004) and data on isotopic geothermometry (Dubinina et al., 2007) suggest that the exothermal character of the olivine hydration reaction does not any significantly affect the heat regime in the Hess crust. For example, at the Rainbow field, at which high-temperature emanations of hydrothermal solutions occur, the main heat donor is likely magmatic activity related to the root parts of the circulation system. It is thus reasonable to assume that the exothermal effect of the serpentinization reaction cannot act as the main heat source for accompanying peridotites in hydrothermal systems. The spatial distribution of magmatic chambers that give rise to gabbro intrusions along the MAR axis likely controls the distribution pattern and dynamic and morphological parameters of hydrothermal circulation systems in slow-spreading ridges (Fontaine et al., 2006). Magmatic chambers beneath slow-spreading ridges may be of significant size. For example, seismic profiling data suggest that magmatic chambers 21–28 km^2 in size occur beneath MAR at 37°17′N at a depth of 3 km from the seafloor surface (Singh et al., 2006). In the context of the problem discussed herein, it is important to mention that geophysical evidence testifies to the occurrence of an array of large faults that bound the rift valley in this MAR segment and possibly reach magmatic chambers beneath the MAR axial zone (Singh et al., 2006).

The large-scale uplift of deep-sitting rocks in the MAR crest zone is favored by the occurrence of extensive exposures of serpentinized mantle peridotites in this zone. In fact, this phenomenon is a principally important empirical indicator of slow-spreading MOR. Data obtained on the succession of hydrothermal minerals formed in MAR peridotites at the Kane Fracture Zone (23°N at MAR) led Andreany et al. (2007) to conclude that these rocks interact with seawater-derived fluid at temperatures from 350 to <150°C, when mantle rocks are exhumed from depths of 8 to <2 km. According to (Andreany et al., 2007), the water of hydrothermal fluids is completely spent on peridotite hydration at significant depths, and this precludes the development of convective hydrothermal cells. Evidence for the uplift of deep crustal rocks in the MAR crest zone is also provided in (Rosner et al., 2007), in which the authors analysis the character of variations in vein associations in rocks of the plutonic complexes that are formed during their ascent and interacting with seawater-derive fluid. Dubinina et al. (2007) published isotopic–geochemical data on the material of aragonite–brucite spires at the Lost City field that indicate that the hydrothermal fluid of this field filtered through already-hydrated (serpentinized) rocks of the Atlantis peridotite massif. It is thus reasonable to conclude that both the results of our simulations and the empirical data presented above indicate that exhumed serpentine blocks is a necessary component of an active hydrothermal circulation system in slow-spreading MOR.

All active hydrothermal systems discovered so far in the Hess crust are hosted in serpentinites composing so-called oceanic core complexes. In addition to peridotites, these complexes consist of gabbroids, vein trondhjemites, and diabases. Large peridotite massifs in which active hydrothermal fields were discovered in the Atlantic are exposed at the seafloor surface in MAR segments that show indications of faulting related to detachment faults. These tectonic features are typical of all known hydrothermal fields at MAR related to serpentinites: Ashadze (*Shipboard…*, 2007), Logachev (Bogdanov et al., 2002; *Shipboard…*, 2007), Lost City (Blackman et al., 2002), and Rainbow (Fouquet et al., 1997).

CONCLUSIONS

The results of our simulations of the phase transformations during the hydrothermal alteration of MOR peridotites led us to propose a geodynamic model for the development of hydrothermal systems related to peridotites in slow-spreading ridges. This model takes into account the principal phases of the compositional and tectonic evolution of the Hess crust. According to the model, low-density serpentinite material formed at crustal depths of about 3.5–4.5 km has an excess volume compared to the pristine unaltered peridotites, and this results in the uplift of this material to upper crustal levels. This processes is associated with faulting of the rigid and cold lithosphere of slow-spreading ridges. The detachment fault arrays produced thereby drain lower crustal magmatic chambers and trigger the emplacement of shallow-depth gabbro intrusions. As a result, conditions favorable for the "startup" of a hydrothermal circulation system are created in the serpentinite slab brought to the seafloor surface (Fig. 9).

In conclusion it can be stated that the development of active hydrothermal systems in slow- and ultraslow-spreading mid-oceanic ridges is closely related to magmatic and tectonic processes in the crest zones of these ridges and reflects the specifics of magmatic melt transportation through the cold and rigid oceanic lithosphere.

ACKNOWLEDGMENTS

The authors thank B.A. Bazylev (Vernadsky Institute of Geochemistry and Analytical Chemistry, Russian Academy of Sciences) for help in evaluating the original mineralogical and chemical composition of typical spinel harzburgite. This study was supported by the Russian Foundation for Basic Research (project nos. 06-05-64003 and 08-05-00164a) and the program of the Presidium of the Russian Academy of Sciences "Fundamental Problems of Oceanology: Physics, Geology, Biology, and Ecology" (section "Interaction

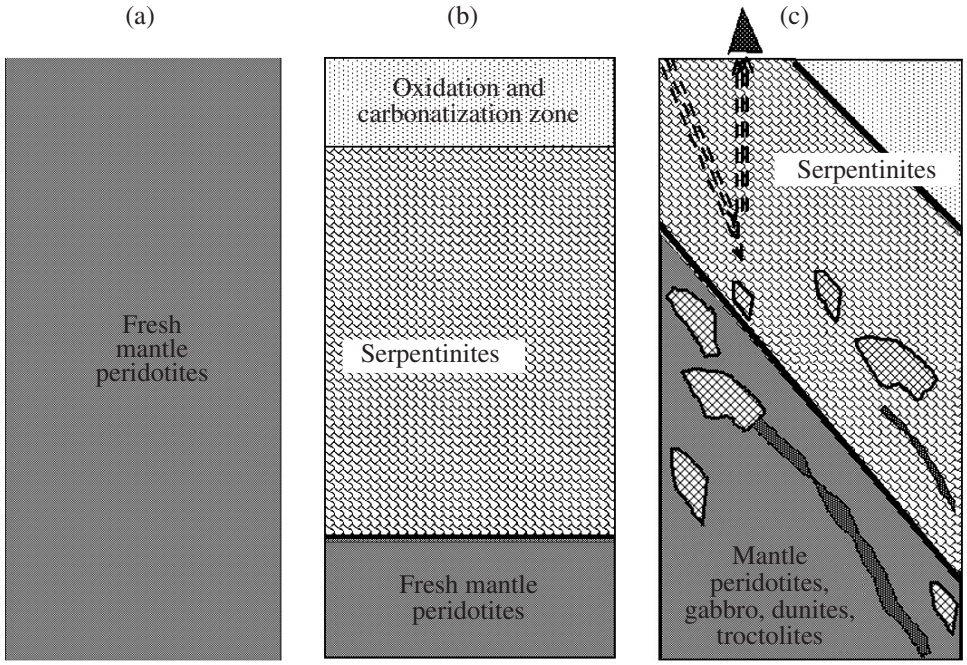

Fig. 9. Schematic geodynamic representation of peridotite evolution in the Hess crust.

Major evolutionary phases that led to the initiation of the hydrothermal process were as follows: (a) development of a mantle diapir of fresh peridotite in the oceanic crust; (b) transformations of mantle peridotites during their interaction with seawater and seawater-derived fluids; (c) tectonic displacement of serpentinites along a detachment fault toward the seafloor surface, origin of gabbroid plutons, and initiation of active hydrothermal circulation.

between Magmatic and Hydrothermal Systems in the Oceanic Lithosphere and Mineral Resources").

REFERENCES

1. P. Aagaard and H. C. Helgeson, "Thermodynamic and Kinetic Constraints on Reaction Rates among Minerals and Aqueous Solutions: I. Theoretical Considerations," Am. J. Sci. **282**, 237–285 (1982).
2. V. A. Alekseev, "Equations for the Dissolution Reaction Rates of Montmorillonite, Illite, and Chlorite," Geokhimiya, No. 8, 842–853 (2007) [Geochem. Int. **45**, 770–780 (2007)].
3. V. A. Alekseev, "Kinetics of the Reaction of Rock-Forming Minerals with Aqueous Solutions," in *Geological Evolution and Self-Organization of the Water–Rock System. Vol. 1. Water–Rock System in the Earth's Crust: Interaction, Kinetics, Equilibrium, and Modeling*, Ed. by S. L. Shvartsev (SO RAN, 2005) [in Russian].
4. D. E. Allen and W. E. Seyfried, Jr., "Serpentinization and Heat Generation: Constraints from Lost City and Rainbow Hydrothermal Systems," Geochim. Cosmochim. Acta. **68**, 1347–1354 (2004).
5. J. C. Alt and W. C. Shanks, "Serpentinization of Abyssal Peridotites from the MARK area, Mid-Atlantic Ridge: Sulfur Geochemistry and Reaction Modeling," Geochim. Cosmochim. Acta **67**, 641–653 (2003).
6. M. Andreani, C. Mevel, A.-M. Boullier, et al., "Dynamic Control on Serpentine Crystallization in Veins: Constraints on Hydration Processes in Oceanic Peridotites," Geochem. Geophys. Geosyst. **8** (2), Q02012 (2007), doi:10.1029/2006GC001373.
7. E. T. Baker, H. N. Edmonds, and P. J. Michael, "Hydrothermal Venting in Magma Deserts: the Ultraslow Spreading Gakkel and Southwest Indian Ridges," Geochem. Geophys. Geosyst. **5** (8), Q 08002 (2004), doi: 10.1029/2004G000712.
8. F. Barriga, A. Dias, A. Marques, et al., "Replacement Processes in Volcanogenic Massive Sulfide Deposits: The Key to Giant Orebodies," Geol. Soc. Am. Annu. Meet. 15–19 (2002).
9. B. A. Bazylev, "Metamorphism of Ultrabasites from the Atlantis Fracture Zone, Atlantic Ocean: Evidnece of Deep Water Penetration in the Oceanic Lithosphere," Dokl. Akad. Nauk **323**, 741–743 (1992).
10. B. A. Bazylev, "Evolution of the Avaruite-Bearing Mineral Assemblage in the Peridotites from 15°20′ Fracture Zone, Atlantic Ocean, as One of the Occurrences of the Oceanic Metamorphism," Ross. Zh. Nauk Zemle **2** (3/4), 279–295 (2000).
11. B. A. Bazylev, *Extended Abstract of Doctoral Dissertation in Geology and Mineralogy* (GEOKhI RAN, Moscow, 2003).
12. M. E. Berndt, D. E. Allen, and W. E. Seyfried, "Reduction of CO_2 during Serpentinization of Olivine at 300°C and 500 bar," Geology **24**, 351–354 (1996).
13. D. K. Blackman, J. A. Karson, D. S. Kelley, et al., "Geology of the Atlantis Massif (Mid-Atlantic Ridge, 30°N): Implications for the Evolution of an Ultramafic Oceanic

Core Complex," Mar. Geophys. Res. **23**, 443–469 (2002).

14. Yu. A. Bogdanov, N. S. Bortnikov, I. V. Vikent'ev, et al., "Mineralogical–Geochemical Peculiarities of Hydrothermal Sulfide Ores and Fluids in the Rainbow Field Associated with Serpentinites, Mid-Atlantic Ridge (36°14′N)," Geol. Rudn. Mestorozhd. **44** (6), 510–542 (2002) [Geol. Ore Dep. **44**, 444–473 (2002)]
15. N. S. Bortnikov, I. V. Vikentyev, I. V. Chernyshov, et al., "Lead Isotope Systematics in Sulfides from Modern Hydrothermal Vents: A Comparison of Mid-Ocean and Back Arc Setting (Pacific)," Mineral. Mag. **58a**, 107–108 (1994).
16. H. Bougault, J. Charlou, Y. Fouquet, et al., "Fast and Slow Spreading Ridges: Structure and Hydrothermal Activity, Ultramafic Topographic Highs, and CH_4 Output," J. Geophys. Res. **98** (B6), 9643–9651 (1993).
17. S. Brantley, "Reaction Kinetics of Primary Rock-Forming Minerals under Ambient Conditions," in *Treatise on Geochemistry* (Elsevier, Amsterdam, 2004), Vol. 5, 73–118.
18. M. Cannat, Y. Lagabrielle, H. Bougault, et al., "Ultramafic and Gabbroic Exposures at the Mid-Atlantic Ridge: Geologic Mapping in the 15°N Region," Tectonophysics **279**, 193–213 (1997).
19. J. Caruso and J. V. Chernosky, "The Stability of Lizardite," Can. Mineral. **17**, 757–769 (1979).
20. J. Charlou, L. Dmitriev, H. Bougault, et al., "Hydrothermal CH_4 between 12°N and 15°N over the Mid-Atlantic Ridge," Deep Sea Res. **35**, 121–131 (1988).
21. J. Charlou, J. P. Donval, Y. Fouquet, et al., "Geochemistry of High H_2 and CH_4 Vent Fluids Issuing from Ultramafic Rocks at the Rainbow Hydrothermal Field (36°14′N, MAR)," Chem. Geol. **191**, 345–359 (2002).
22. J. Charlou, J. P. Donval, P. Jean-Baptiste, et al., "Abiogenic Petroleum Generated by Serpentinization of Oceanic Mantellic Rocks," AAPG Res. Conf. Calgary (Canada, 2005), p. 44.
23. Y. Chen and S. Brantley, "Dissolution of Forsteritic Olivine at 65°C and 2 < pH < 5," Chem. Geol. **165**, 267–281 (2000).
24. J. V. Chernosky, R. G. Berman, and L. T. Bryndzia, "Stability, Phase Relations, and the Thermodynamic Properties of Chlorite and Serpentine Group Minerals," in *Hydrous Phyllosilicates*, Ed. by S. W. Bailey. Rev. Mineral. **19**, 295–346 (1988).
25. J. V. J. Chernosky, *An Experimental Investigation of the Serpentine and Chlorite Group Minerals in the System MgO–Al_2O_3–SiO_2–H_2O* (Mass. Inst. of Technol, Cambridge, 1973).
26. H. J. B. Dick, J. Lin, and H. Shouten, "An Ultraslow-Spreading Class of Ocean Ridges," Nature **426**, 405–412 (2003).
27. H. J. B. Dick, P. S. Meyer, R. S. Bloomes, et al., "Lithostratigraphic Evolution of an In-Situ Section of Oceanic Layer 3," Proc. Ocean Drill. Progr. Sci. Res. **118**, 439–538 (1991).
28. H. J. B. Dick, J. H. Natland, and B. Ildefonse, "Past and Future Impact of Deep Drilling in the Oceanic Crust and Mantle," Oceanography **19**, 72–80 (2006).
29. E. V. Dobrovol'skii, *Extended Abstract of Candidate's Dissertation in Geology and Mineralogy* (IGN AN USSR, Kiev, 1978).
30. E. O. Dubinina, I. V. Chernyshev, N. S. Bortnikov, et al., "Isotopic–Geochemical Characteristics of the Lost City Hydrothermal Field," Geokhimiya, No. 11, 1223–1236 (2007) [Geochem. Int. **45**, 1124–1130 (2007)].
31. B. W. Evans, "The Serpentinite Multisystem Revisited: Chrysotile is Metastable," Int. Geol. Rev. **46**, 479–506 (2004).
32. B. W. Evans, W. Johannes, Y. Oterdoom, et al., "Stability of Chrysotile and Antigorite in the Serpentine Multisystem," Schweiz. Mineral. Petrogr. Mitt. **56**, 79–93 (1976).
33. *Expedition 304/305 Scientists, Site U1309*, Ed. by D. K. Blackman, B. Ildefonse, B. E. John, Y. Ohara, et al., Proc. IODP, 304/305: College Station TX (Integrated Ocean Drilling Program Management International, 2006).
34. F. Fontaine, M. Cannat, J. Escartin, et al., "Characteristics of Hydrothermal Convection in Inclined Layers: Implications for Hydrothermal Activity at Slow-Spreading Axis," Eos Trans. AGU **87**, Abstract B31B-1109 (2006).
35. Y. Fouquet, J. Charlou, H. Ondreas, et al., "Discovery and First Submersible Investigations on the Rainbow Hydrothermal Field on the MAR (36°14′N)," Eos Trans. **78**, 832 (1997).
36. G. Fruh-Green, D. S. Kelley, S. M. Bernasconi, et al., "30000 Years of Hydrothermal Activity at the Lost City Vent Field," Science **301**, 495–498 (2003).
37. D. V. Grichuk, "Thermodynamic Model of Hydrothermal System in Hyperbasites," in *Proceedings of 16th International School of Marine Geology* (Moscow, 2005), pp. 272–273 [in Russian].
38. D. V. Grichuk, *Thermodynamic Models of Submarine Hydrothermal Systems* (Nauchnyi Mir, Moscow, 2000) [in Russian].
39. H. C. Helgeson, "Evaluation of Irreversible Reactions in Geochemical Processes Involving Minerals and Aqueous Solutions: I. Thermodynamic Relations," Geochim. Cosmochim. Acta **32**, 569–592 (1968).
40. H. C. Helgeson, J. Delany, D. K. Bird, "Summary and Critique of the Thermodynamic Properties of Rock-Forming Minerals," Am. J. Sci. **278A**, 1–229 (1978).
41. T. J. B. Holland and R. Powell, "An Internally Consistent Thermodynamic Data Set for Phases of Petrologic Interest," J. Metamorph. Geol. **16**, 309–343 (1998).
42. W. Johannes, "Experimental Investigation of the Reaction Forsterite + H_2O = Serpentine + Brucite," Contrib. Mineral. Petrol. **19**, 309–315 (1968).
43. J. A. Karson, "Internal Structure of Oceanic Lithosphere: A Perspective from Tectonic Windows," in *Faulting and Magmatism at Mid-Ocean Ridges*, Ed. by W. Buck, P. T. Delaney, J. A. Karson, and Y. Lagabrielle, Geophys. Monogr. **106**, 177–218 (1998).
44. D. S. Kelley and J. R. Delaney, "Two-Phase Separation and Fracturing in Mid-Ocean Ridge Gabbros at Temperatures Greater than 700°C," Earth Planet. Sci. Lett. **83**, 53–66 (1987).
45. D. S. Kelley, J. A. Karson, D. K. Blackman, et al., "An Off-Axis Hydrothermal Vent Field near Mid-Atlantic Ridge at 30°N," Nature **412**, 145–149 (2001).

46. D. S. Kelley, J. A. Karson, G. Fruh-Green, et al., "A Serpentinite-Hosted Ecosystem: The Lost City Hydrothermal Field," Science **307**, 1420–1422 (2005).

47. L. Kump, S. L. Brantley, and M. A. Arthur, "Chemical Weathering, Atmospheric CO_2 and Climate," Earth Planet. Sci. Rev. **28**, 611–667 (2000).

48. A. C. Lasaga, "Transition State Theory," in *Kinetics of Geochemical Processes*, Ed. by A. C. Lasaga and R. J. Kirkpatrick, Rev. Mineral. **8**, 135–169 (1981).

49. A. F. Marques, F. J. Barriga, V. Chavagnac, et al., "Mineralogy, Geochemistry and Nd Isotope Composition of the Rainbow Hydrothermal Field, Mid-Atlantic Ridge," Mineral. Deposita **41**, 52–67 (2006).

50. R. A. Mayanovic, A. J. Anderson, W. A. Bassett, et al., "The Structure of REE Aqua and Chloroaqua Complexes in Hydrothermal Fluids," in *Proceedings of the Goldschmidt Conference, Cologne, Germany, 2007* (Cologne, 2007), A642.

51. T. M. McCollom and E. Shock, "Fluid-Rock Interactions in the Lower Oceanic Crust: Thermodynamic Models of Hydrothermal Alteration," J. Geophys. Res. **103** (B1), 547–575 (1998).

52. P. J. Michael, C. H. Langmuir, H. J. B. Dick, et al., "Magmatic and Amagmatic Sea Floor Spreading at the Slowest Mid-Ocean Ridge: Gakkel Ridge, Arctic Ocean," Nature **423**, 956–96 (2003).

53. M. V. Mironenko, N. N. Akinfiev, and T. Yu. Melikhova, "GEOSHEQ—A Complex of Thermodynamic Modeling of Geochemical Systems," Vestn. OGGGN RAN **5** (15), 96–97 (2000).

54. M. J. Mottl, "Metabasalts, Axial Hot Springs and the Structure of Hydrothermal Systems at Mid-Ocean Ridges," Geol. Soc. Amer. Bull. **94**, 161 (1983).

55. P. Nonnotte, G. Ceuleneer, and M. Benoit, "Genesis of Andesitic-Boninitic Magmas at Mid-Ocean Ridges by Melting of Hydrated Peridotites: Geochemical Evidence from DSDP Site 334 Gabbronorites," Earth Planet. Sci. Lett. **236**, 632–653 (2005).

56. D. S. O'Hanley and F. J. Wicks, "Conditions of Formations of Lizardite, Chrysotile and Antigorite, Cassiar, British Columbia," Can. Mineral. **33**, 753–773 (1995).

57. O. S. Pokrovsky and J. Schott, "Kinetics and Mechanism of Forsterite Dissolution at 258°C and pH from 1 to 12," Geochim. Cosmochim. Acta **64**, 3313–3325 (2000).

58. G. Proskurowski, M. D. Lilley, D. S. Kelley, et al., "Low Temperature Volatile Production at the Lost City Hydrothermal Field: Evidence from a Hydrogen Stable Isotope Geothermometer," Chem. Geol. **229**, 331–343 (2006).

59. Report of 24th Cruise of the R/V *Professor Logachev* (PMGRE, Lomonosov: 2004).

60. P. A. Rona, L. Widenfalk, and K. Bostrum, "Serpentinized Ultramafics and Hydrothermal Activity at the Mid-Atlantic Ridge Crest near 15°N," J. Geophys. Res. **92**, 1417–1427 (1987).

61. M. Rosner, W. Bach, B. Peucker-Ehrenbrink, et al., "Carbonate and Anhydrite Veins from Altered Gabbroic Oceanic Crust (Atlantis Massif, MAR 30°N)," in *Proceeding of Goldschmidt Conference Abstracts, Cologne, Germany, 2007* (Cologne, 2007), p. A853.

62. Z. D. Sharp and J. D. Barnes, "Water-Soluble Chlorides in Massive Seafloor Serpentinites: A Source of Chloride in Subduction Zones," Earth Planet. Sci. Lett. **226**, 243–254 (2004).

63. *Shipboard Scientific Party, Serpentine. Scientific Cruise Report* (Iferemer-Centre de Brest, 2007).

64. "Shipboard Scientific Party. Drilling Mantle Peridotite along the Mid-Atlantic Ridge from 14° to 16°N," in *Ocean Drilling Program. Leg 209 Preliminary Report. Texas A&M University* (College Station, TX, USA, 2003), p. 160.

65. E. Shock, H. C. Helgeson, and D. A. Sverjensky, "Calculation of the Thermodynamic and Transport Properties of Aqueous Species at High Pressures and Temperatures: Standard Partial and Molar Properties of Inorganic Neutral Species," Geochim. Cosmochim. Acta **53**, 2157–2183 (1989).

66. E. Shock, D. C. Sassani, M. Willis, et al., "Inorganic Species in Geologic Fluids: Correlations among Standard Molal Thermodynamic Properties of Aqueous Ions and Hydroxide Complexes," Geochim. Cosmochim. Acta **61**, 907–950 (1997).

67. P. S. Sidhu, R. J. Gilkes, R. M. Coenell, et al., "Dissolution of Iron Oxides and Oxyhydroxides in Hydrolic and Perhydrolic Acids," Clays Clay Miner. **29**, 269–276 (1981).

68. S. A. Silantyev and B. V. Belyatskii, "Concentration and Isotopic Composition of Strontium, Lead, and Neodymium in the Mantle Restites of the Mid-Atlantic Ridge and their Relation with Endogenic and Exogenic Factors of the Oceanic Lithosphere," in *Proceedings of 15th Vinogradov Symposium on Isotope Geochemistry* (Moscow, 1998), pp. 260–261 [in Russian].

69. S. A. Silantyev, A. A. Novoselov, M. V. Mironenko, et al., "Geochemical Features and Thermodynamic Modeling of Hydration and Carbonatization of Mantle Peridotites in the Inner Corner Highs of MAR: An Example of 15°04′ N (Bugo Diapir)," in *Working Conference of Russian Branch of the InterRidge International Project, St. Petersburg, Russia, 2005* (St. Petersburg, 2005), p. 14 [in Russian].

70. S. A. Silantyev, A. A. Novoselov, M. V. Mironenko, et al., "Redox Regime of Hydration of the Hess-Type Crust," in *Working Conference of Russian Department of the InterRidge International Project, St. Petersburg, Russia, 2003* (Moscow, 2003), p. 42 [in Russian].

71. S. Silantyev, E. Krasnova, N. Bortnikov, et al., "Structure of the Oceanic Inner Complexes as Key to the Reconstructing of Magmatic and Tectonic Evolution of the Lithosphere of Slow-Spreading MAR: Evidence from the Atlantic Massif, MAR, 30°N," in *Proceedings of Working Conference of Russian Department of InterRidge International Project on Geochemical, Petrological, and Geophysical Segmentation of MAR and its Relation with Geodynamic Parameters of Accretion of the Oceanic Lithosphere, Moscow, Russia, 2007* (Moscow, 2007), pp. 46–48 [in Russian].

72. S. A. Silantyev, M. V. Mironenko, B. A. Bazylev, and Yu. V. Semenov, "Metamorphism Related to Hydrothermal Systems of Mid-Ocean ridges; Experience of Thermodynamic Modeling," Geokhimiya, No. 7, 1015–1034 (1992).

73. S. A. Silantyev, R. Magakyan, S. K. Zlobin, et al., "New Data on the Structure of the Oceanic Crust of the Central Atlantic, 15°20; Fracture Zone: Preliminary results of

16th Cruise of the R/V *Akademik Boris Petrov*, Second Stage," Dokl. Akad. Nauk SSSR **318** (1), 172–175 (1991).

74. S. C. Singh, W. C. Crawford, H. Carton, et al., "Discovery of a Magma Chamber and Faults beneath a Mid-Atlantic Ridge Hydrothermal Field," Nature. **442**, 1029–1032 (2006).
75. N. H. Sleep, "Thermal Structure and Kinematics of Mid-Ocean Ridge Axes: Some Implications to Basaltic Volcanism," Geophys. Res. Lett. **5**, 426–428 (1978).
76. J. E. Snow and L. Reisberg, "On Isotopic Systematics of MORB Mantle: Results from Altered Abyssal Peridotites," Earth Planet. Sci. Lett. **133**, 411–421 (1995).
77. J. E. Thomas, R. St. C. Smart, and W. M. Skinner, "Kinetic Factors for Oxidative and Non-Oxidative Dissolution of Iron Sulfides," Mineral. Engin. **13**, 1149–1159 (2000).
78. M. K. Tivey, "Generation of Seafloor Hydrothermal Vent Fluids and Associated Mineral Deposits," Oceanography **20**, 50–65 (2007).
79. P. Vieillard, S. Ramirez, A. Bouchet, et al., "Alteration of the Callovo-Oxfordian Clay from Meuse-Haute Marne Underground Laboratory (France) by Alkaline Solution: II. Modeling of Mineral Reactions," Appl. Geochem. **19**, 1699–1709 (2004).
80. I. V. Vikent'ev, *Genesis and Metamorphism of Sulfide Ores* (Nauchnyi Mir, Moscow, 2004) [in Russian].
81. J. Wilson, D. Savage, J. Cuadros, et al., "The Effect of Iron on Montmorillonite Stability: I. Background and Thermodynamic Considerations," Geochim. Cosmochim. Acta. **70**, 306–322 (2006).
82. R. A. Wogelius and J. V. Walther, "Olivine Dissolution Kinetics at Near-Surface Conditions," Chem. Geol. **97**, 101–112 (1992).
83. T. J. Wolery and C. F. Jove-Colon, "Qualification of Thermodynamic Data for Geochemical Modeling of Mineral–Water Interactions in Dilute Systems," in *Rep. ANL-WIS-GS-000003 REV 00* (U.S. Dep. Energy, Washington, 2004), p. 212.
84. M. Y. Zolotov and M. V. Mironenko, "Timing of Acid Weathering on Mars: A Kinetic-Thermodynamic Assessment," J. Geophys. Res. **112**, E07006 (2007), doi:10.1029/2006JE002882.